Dark localized structures in a cavity filled with a left-handed material

Mustapha Tlidi,[1] Pascal Kockaert,[2] and Lendert Gelens[3]
[1]*Optique non linéaire théorique, Université Libre de Bruxelles, CP 231, Campus Plaine, B-1050 Bruxelles, Belgium*
[2]*OPERA-photonique, Université Libre de Bruxelles, CP 194/5, 50, Av. F. D. Roosevelt, B-1050 Bruxelles, Belgium*
[3]*Applied Physics Research Group (APHY), Vrije Universiteit Brussel, Pleinlaan 2, B-1050 Brussel, Belgium*
(Received 21 February 2011; published 8 July 2011)

We consider a nonlinear passive optical cavity filled with left-handed and right-handed materials and driven by a coherent injected beam. We assume that both left-handed and right-handed materials possess a Kerr focusing type of nonlinearity. We show that close to the zero-diffraction regime, high-order diffraction allows us to stabilize dark localized structures in this device. These structures consist of dips in the transverse profile of the intracavity field and do not exist without high-order diffraction. We analyze the snaking bifurcation diagram associated with these structures. Finally, a realistic estimation of the model parameters is provided.

DOI: 10.1103/PhysRevA.84.013807 PACS number(s): 42.65.Tg, 42.25.Bs, 42.60.Mi

I. INTRODUCTION

During the last decade, the study of optical properties of left-handed materials (LHMs), often referred to as metamaterials, has attracted considerable attention both from fundamental as well as from applied point of views (see recent special issue [1]). Particular attention has been paid to the characterization of their linear properties and their fabrication [2–8]. Several studies reveal the importance of nonlinear phenomena in the propagation of light in LHMs [9–12]. More recently, the combination of a layer of LHM together with nonlinear propagation in a second layer of right-handed material (RHM) (see Fig. 1) has shown to offer possibilities to design devices where the mean diffraction is close to zero [13,14]. When operating around the zero-diffraction regime and by taking into account the nonlocal properties of light propagation in such a double-layered (LHM+RHM) optical cavity, the spatiotemporal evolution of the intracavity field can be described by the following dimensionless partial differential equation [15]:

$$\frac{\partial A}{\partial t} = A_i - (1 + i\Delta)A + i\Gamma |A|^2 A + i\delta \tilde{\nabla}_\perp^2 A + \left(i\theta - \frac{\delta^2}{2}\right)\tilde{\nabla}_\perp^4 A, \quad (1)$$

where A is the slowly varying envelope of light within the ring cavity, A_i is the amplitude of the injected field, Δ is the normalized cavity detuning parameter, and Γ is the normalized nonlinear Kerr coefficient. The Laplace operator that acts on the transverse plane is $\tilde{\nabla}_\perp^2 = (\partial_{xx}^2 + \partial_{yy}^2)/k_0^2$, with k_0 the wave number of the light. The time has been scaled as in [15]. The effective diffraction coefficient is denoted by δ. As explained in [13], the coefficient δ can be tuned by adjusting the relative width of the RHM and the LHM layers. The coefficient θ accounts for the higher-order spatial effects in the cavity.

In this work, we show that combining a RHM and LHM allows us to stabilize both one-dimensional (1D) and two-dimensional (2D) dark localized structures (DLS). These DLS consist of a slug of a patterned state embedded in a homogeneous steady state, i.e., they arise as dips in a homogeneous steady state of higher intensity. The number of dips and their spatial distribution in the transverse plane of the cavity is determined by the initial conditions. We construct the bifurcation diagram associated with these structures and show that they exhibit a homoclinic snaking type of behavior.

In the absence of the bi-Laplacian term ($\nabla_\perp^4 A = 0$) in Eq. (1), we recover the Lugiato-Lefever model [16]. It has been shown that the Lugiato-Lefever equation admits stable 1D and 2D bright localized structures [17,18]. These localized structures can be seen as intensity peaks on a homogeneous steady state of lower intensity. A theoretical study of the model [Eq. (1)] without the diffusion term, i.e., $\delta^2\nabla_\perp^4 A$, reveals that high-order diffraction can give rise to a degenerate modulational instability where two separate unstable wavelengths simultaneously appear [14]. Close to the first modulation instability threshold, stable bright localized structures are created. These bright localized structures in nonlinear optical cavities, also called cavity solitons, have been experimentally demonstrated using semiconductor microcavities [19] or liquid crystal light valves with optical feedback [20]. More recently, such cavity solitons have been reported experimentally in one dimension in a normal dispersive all-fiber ring resonator [21]. In the case of a fiber ring resonator, diffraction is replaced by chromatic dispersion. In this context, localized structures are often called temporal cavity solitons. Localized structures have been shown to have potential applications in the all-optical control of light and in the optical storage and processing of information [19]. Recent overviews can be found in Refs. [22–26]. So far, however, the width of these localized structures is limited by diffraction, presenting an important limitation on the data capacity in optical storage schemes based on localized structures. The inclusion of a LHM element in microcavities allows us to operate close to a low-diffraction regime, which leads to a dramatic reduction of the width of localized structures [14]. Close to the zero-diffraction regime, higher-order spatial derivatives have to be included in order to correctly capture the dynamics of the system [see Eq. (1)]. Note that localized structures (also called dissipative solitons) in the regime close to zero dispersion have also been predicted in other nonlinear systems, such as Bose-Einstein condensates [27]. Diffraction engineering also occurs in resonators filled with photonic crystals, where index modulation has been proposed to overcome the diffraction limit of midband solitons [28].

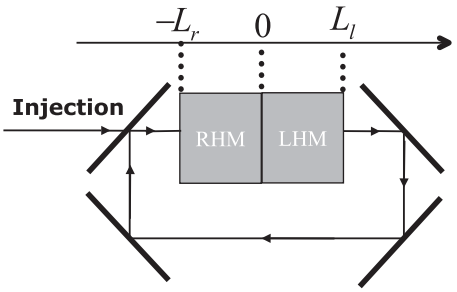

FIG. 1. Schematic setup of a ring cavity filled with right-handed and left-handed materials. The cavity is driven by a coherent external injected beam. The lengths of the left- and right-handed layers are L_l and L_r, respectively.

The paper is organized as follows. In Sec. II, we discuss the spatial dispersion in a left-handed material and provide an estimation of the model parameters in Eq. (1). In Sec. III, we present a summary of a linear stability analysis. In Sec. IV, we show that the presence of high-order diffraction allows us to stabilize dark localized structures in both one and two spatial dimensions. Next, we discuss the snaking phenomenon associated with these structures. Finally, in Sec. V, we conclude.

II. SPATIAL DISPERSION IN A LEFT-HANDED MATERIAL

In Ref. [15], it is mentioned how to calculate θ on the basis of the spatial dispersion coefficient η of the material. However, this coefficient

$$\eta = \frac{1}{4!}\frac{\partial^4 \beta_0^2}{\partial {k_x}^4} \tag{2}$$

cannot be defined without further assumptions about the geometry of the material, i.e., its spatial symmetries as well as its structure at the wavelength scale (a few nanometers up to 1 μm in the optical range).

In Appendix A, we consider one of the simplest cases of interest, for which the structure presents the group symmetry 4/mmm (as the one studied in [29]), and the nonlocal interaction between light and this structure is given by an homogeneous response [30]

$$\frac{e^{-\mu|\mathbf{r}'-\mathbf{r}|}}{|\mathbf{r}'-\mathbf{r}|}, \tag{3}$$

where $\mathbf{r}$ and $\mathbf{r}'$ denote, respectively, the source and the test points, and where the parameter μ determines the effective range of the nonlocality. Such a nonlocal interaction corresponds in the Fourier domain to a dielectric susceptibility given by

$$\tilde{\hat{\chi}} = \frac{\chi_0}{k^2 + \mathcal{L}(\omega)}, \tag{4}$$

where k is the wave number, ω is the pulsation, and $\mathcal{L}(\omega) = \mu^2$ accounts for the frequency response of the material. The nonlocality extends over a range given by the mean interaction radius [see Eqs. (A3)–(A5) for details].

$$R = \frac{1}{\mathrm{Re}[\sqrt{\mathcal{L}(\omega)}]}. \tag{5}$$

Combining the analytic expression for the susceptibility with the assumption that the material is left handed leads to a set of one equation and two inequalities. This set of relations can be calculated in the vicinity of a resonance characterized by a Lorentz peak

$$\mathcal{L}(\omega) = \left(\omega_\mathrm{r}^2 - \omega^2 - i\gamma_\mathrm{r}\omega\right)/c^2, \tag{6}$$

with ω_r and $1/\gamma_\mathrm{r}$, respectively, the central pulsation and the width of the resonance peak. Provided that the resonance is sharp enough, $\gamma_\mathrm{r} \ll \omega_\mathrm{r}$, the calculation presented in Appendix A leads to the conclusions that $\eta \approx (n_\mathrm{r}^2 - 1)/k_\mathrm{r}$ [see Eq. (A39)], and that the interaction radius is mainly linked to the width of the resonance:

$$R \approx c\sqrt{\frac{2}{\gamma_\mathrm{r}\omega_\mathrm{r}}}. \tag{7}$$

In these expressions, n_r denotes the refractive index and $k_\mathrm{r} = \omega_\mathrm{r} n_\mathrm{r}/c$. On the left-handed side of the resonance, $n_\mathrm{r} = n_\mathrm{L} < 0$, which implies that the available range of values for η is varying from a few percents of k_r^{-2} up to k_r^{-2}. In a cavity with a negligible spatial dispersion in the right-handed material, a finesse $\mathcal{F}$, and a thickness of the left-handed material l_L, for $\mathcal{F} l_L/\lambda_L \approx 100$ and $n_L^2 \approx 1$, we find an effective dispersion coefficient in reduced units:

$$\bar{\theta} \approx \left(1 - n_L^2\right)\frac{\mathcal{F}}{2}\frac{l_L}{\lambda_L}, \tag{8}$$

varying between 0.1 and 1. All the results presented in this paper were obtained in this range of values for $\bar{\theta}$.

III. LINEAR STABILITY ANALYSIS

The homogeneous steady states A_s of Eq. (1) are given by $I_i = [1 + (\Delta - \Gamma I_s)^2]I_s$. The transmitted intensity $I_s = |A_s|^2$ as a function of the input intensity $I_i = |A_i|^2$ is monostable for $\Delta < \sqrt{3}$. Bistable behavior arises for $\Delta > \sqrt{3}$. The homogeneous steady states are not affected by the high-order diffraction terms. However, these terms play an important role in the linear stability analysis with respect to finite wavelength perturbations of the form $\exp(\sigma t + i\mathbf{q}\cdot\mathbf{r}_\perp)$ with $\mathbf{q} = (q_x, q_y)$. The modulation instability occurs when $\sigma = 0$. This leads to the marginal stability curve

$$\left(\theta^2 + \frac{\delta^4}{4}\right)q^8 - 2\delta\theta q^6 + 2[\theta(2\Gamma I_s - \Delta) + \delta^2]q^4 + 2\delta(\Delta - 2\Gamma I_s)q^2 + 1 + \Delta^2 - \Gamma I_s(4\Delta - \Gamma I_s) = 0. \tag{9}$$

The threshold associated with the modulation instability as well as the wavelength of the periodic structure emerging from that threshold can be obtained when $\partial I_s/\partial q = 0$. The results of the linear stability analysis are summarized in Fig. 2. When decreasing the input field intensity I_i, the upper homogeneous steady state becomes unstable at $I_M = |A_M|^2$. At this bifurcation point, the most unstable wavelength is $2\pi/q_M$. When further decreasing I_i, the lower branch of the bistable input-output characteristics is reached which is stable again. Close to the first modulation instability threshold, bright

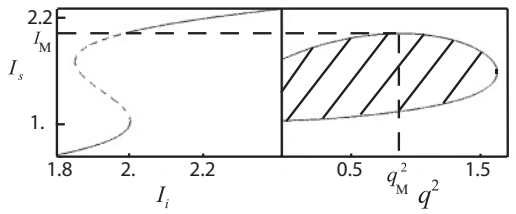

FIG. 2. Bistable input-output characteristics. The dashed curve indicates unstable solutions and the solid lines indicate stable ones. The associated marginal instability curve $I_s = |A_s|^2$ as a function of wave number q^2 is also shown. The hatched area corresponds to an unstable region with respect to modulation instabilities. Parameters are $\Delta = 2$, $\theta = 0.2$, $\Gamma = 1$, and $\delta = 0.5$.

localized structures can exist. Such bright cavity solitons in nonlinear optical cavities based on LHM have been theoretically predicted [14,31]. Note that in the absence of the diffusion term, i.e., $\delta^2\nabla_\perp^4 A$, in Eq. (1), the critical wave number at the onset of the modulation instability affecting the upper branch of the homogeneous steady states is $q_M^2 = \delta/(4\theta)$. This simple expression thus clearly shows that the spontaneous modulation instability requires $\delta\theta > 0$, i.e., δ and θ should have the same sign.

IV. FORMATION OF DARK LOCALIZED STRUCTURES

In this work, we are interested in the situation where two stable solutions coexist and can connect to each other forming a stable DLS. In region A, both homogeneous steady states are stable [see Fig. 3(a)]. Numerical simulations have shown, however, that the lower homogeneous steady state is always favored. Depending on the initial conditions, the system either evolves toward the lower homogeneous steady state or a periodic structure, such that no DLS can exist as a connection between the two stable homogeneous steady states. However, as the patterns are created subcritically, a finite domain of coexistence between stable periodic structures and a stable upper homogeneous steady state is also present. Figure 3(a) shows two such periodic pattern solutions P_n with wavelengths $k_n = 2\pi n/L$, with n an integer defining the number of periods that fit in the domain with size L. In this region, there exists a so-called "pinning region" (region B) where single or multiple dips in the intensity profile can be generated numerically. Examples of such DLS are shown in Fig. 3(c), where only the profiles (1) and (6) represent stable DLS profiles.

In order to analyze the DLS in more detail in 1D, we draw a snaking bifurcation diagram in Fig. 3(b), plotting the "energy" = "normalized number of photons" = $\int dx|A|^2$ as a function of A_i. These solutions are found by using appropriate initial conditions and are then continued in parameter space

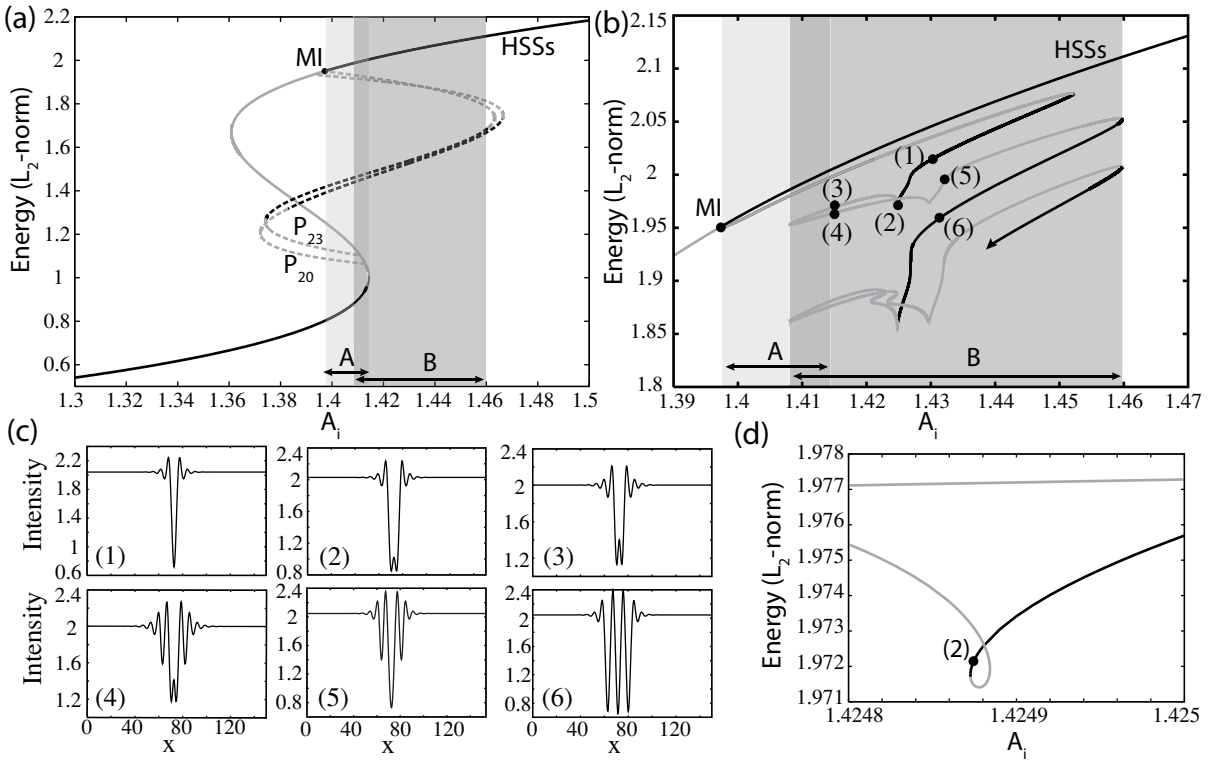

FIG. 3. (a) Bistable input-output characteristics. Dashed curves indicate periodic solutions and solid lines indicate homogeneous steady states. Stable (unstable) solutions are colored in black (gray). (b) Snaking bifurcation diagram of the 1D DLS. (c) Intensity profiles of 1D DLS obtained for input field amplitudes as indicated in (b). (d) Zoom of the bifurcation behavior around the profile (2) indicated in (b). Parameters: $\Delta = 2$, $\theta = 0.2$, $\Gamma = 1$, $\delta = 0.5$, and $L = 153.6$ (with 512 discretization points).

using a Newton method. Periodic boundary conditions are used. A typical snaking diagram, as, e.g., widely studied in the context of the variational Swift-Hohenberg equation [32], consists of two snaking curves; one describes DLS with an odd number of dips and the other corresponds to an even number of dips. The DLS originate at the modulation instability of the homogeneous steady state and are initially unstable. As one moves further along the snaking curve, the DLS become better localized and acquire stability at the turning point where the slope becomes infinite. Afterwards, the DLS begin to grow in spatial extent by adding extra dips symmetrically at either side. This growth is associated with back and forth oscillations across the pinning interval. This behavior is referred to as homoclinic snaking [32–36]. Although both the odd and even branch are present here, to simplify the analysis, we focus only on DLS with an odd number of dips in the intensity profile. Although the snaking curve in Fig. 3(b) is similar to the homoclinic snaking of DLS as, e.g., shown in Ref. [34], one can notice that on the left-hand side of the snaking curve, the growth process is more complicated. In order to nucleate an extra pair of DLS, the system evolves through a more intricate transient with dips showing a double-peaked minima. When decreasing the energy of the stable single DLS [see profile (1)], a double dip in the intensity profile is continuously introduced [see profile (2)]. Afterwards a series of fold bifurcations [see Figs. 3(b) and 3(d)] changes the morphology of the DLS profile until it has evolved to a stable DLS consisting of three dips [see profile (6)]. The presence of such a central defect in the growth process of DLS bears similarity with the recently introduced defect-mediated snaking [35]. However, in contrast to Ref. [35], here the central defect is first removed [see evolution profile (5) to (6)] and the extra rolls are then added at the sides instead of growing from the center.

The added complexity in the snaking curve seems to be connected to the proximity of the saddle-node bifurcation of the lower branch homogeneous steady state such that a region A of coexistence between two stable homogeneous steady states is present. When decreasing the detuning Δ, the lower fold bifurcation and the modulation instability shift to lower values of A_i. Due to the faster change of the position of the fold, however, the width of region A decreases and eventually disappears. In doing so, for $\Delta < 1.91$, the complexity in the snaking branch is no longer present and the more regular homoclinic snaking [32–34] is again recovered. Although beyond the scope of this work, a more detailed investigation of the interplay of the snaking curve with the region of the bistable homogeneous steady state is interesting in its own right and is left for future investigations.

In two spatial dimensions, the number of DLS can clearly be much larger than in 1D. We focus on the situation where 2D DLS are close to one another. They exert mutual forces due to their overlapping oscillatory tails. As the number of DLS increases, the transverse profile of the output electric field exhibits clustering behavior as shown in Fig. 4. As in the 1D case, the number of 2D dips and their spatial distribution depends only on the initial condition used. Examples of 2D DLS are plotted in Fig. 4. Figures 4(a)–4(c) correspond to the real part, and Figs. 4(d)–4(f) to the imaginary part of the intracavity field. All these DLS profiles

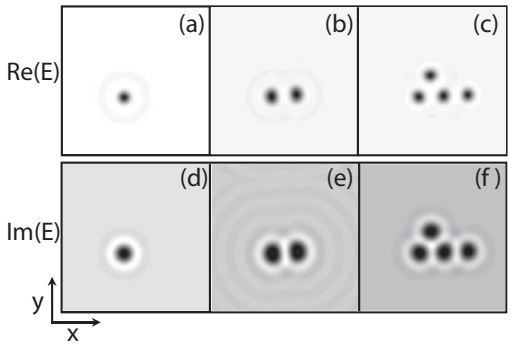

FIG. 4. Examples of 2D multiple DLS obtained for $\Delta = 2$, $\theta = 0.2$, $\Gamma = 1$, $\delta = 0.5$, and $A_i = 1.437$. Minima are colored in black and the grid is 256×256. The domain size of the system in both transverse directions is $L_x = L_y = 89.6$.

are obtained for the same parameter values, and thus, the system exhibits a high degree of multistability. Constructing corresponding snaking curves in 2D is a challenging task, which we do not pursue further here. For an in-depth study of snaking in the 2D Swift-Hohenberg equation, we refer readers to Ref. [36].

V. CONCLUSIONS

In conclusion, we have shown that around the zero-diffraction regime in an optical cavity containing both left- and right-handed materials, one- and two-dimensional dark localized structures can become stable. The stabilization of these structures is the result of high-order diffraction modeled by a bi-Laplacian term with a complex coefficient. We have provided an estimation of this bi-Laplacian term for such a double-layered cavity. In one spatial dimension, a snaking bifurcation diagram has been demonstrated to exist for these solutions, which shows a larger complexity than generally observed in homoclinic snaking. In two dimensions, numerical simulations have demonstrated a similar coexistence of multiple dips in the intensity profile.

ACKNOWLEDGMENTS

M. T. is supported by the Fonds de la Recherche Scientifique F.R.S.-FNRS, Belgium. L. G. acknowledges support by the Research Foundation – Flanders (FWO-Vlaanderen). This work is partly supported by the Belgian Science Policy Office under Grant No. IAP6-10. We thank D. Gomila, G. Van der Sande, and E. Knobloch for useful comments.

APPENDIX: ORDER OF MAGNITUDE ESTIMATION OF THE SPATIAL DISPERSION IN A LEFT-HANDED MATERIAL

In this Appendix, it is our intent to evaluate the order of magnitude of the spatial dispersion parameter η defined in [15]. To this end, the nonlocal behavior is described with the use of a homogeneous model. On the basis of realistic assumptions, we provide a range of values for the spatial dispersion parameter.

1. Preliminary

Before we introduce the model that we used to evaluate the magnitude of the spatial dispersion in a left-handed material, it is probably important to provide a definition for the concept of spatial dispersion. We use the expression "spatial dispersion," as defined by Agranovich and Ginzburg in [37], p. 239] and [38], p. 252], i.e., to denote a dependence of the permittivity tensor on the wave vector. This dependence reflects the nonlocality of the medium: the fact that the displacement field at a given point is induced by the electric field in a neighborhood of this point.

Different models can be used to describe the nonlocal behavior of the material. We will not review all of them, but present the homogeneous one that should provide a good estimate of the spatial dispersion in metamaterials with 4/mmm point symmetry.

2. Symmetry of the subwavelength structure

Refering to Eq. (50) in [15], the parameter of importance to characterize the nonlocal behavior of the material is

$$\eta = \frac{1}{4!}\frac{\partial^4 \beta_0^2}{\partial {k_x}^4}. \tag{A1}$$

This value is obtained under the assumption that the medium is symmetric with respect to a rotation of $\pi/2$ around the propagation axis. This assumption does not hold in certain kinds of metamaterials, such as those based on structures with a "U" shape. However, other structures, like the one presented in [29], are compatible with this assumption. These materials belong to the group symmetry 4/mmm. Therefore, in what follows, we will restrict our analysis to structures of this group.

3. Nonlocal homogeneous response

Different models have been proposed to take into account nonlocal interactions at the microscopic level. In a simple but yet efficient model [39], it is assumed that the nonlocal interaction decreases as

$$\frac{e^{-\mu|\mathbf{r}'-\mathbf{r}|}}{|\mathbf{r}'-\mathbf{r}|}, \tag{A2}$$

where $\mathbf{r}$ and $\mathbf{r}'$ denote, respectively, the source and the test points, and where the parameter μ determines the effective range of the nonlocality.

This model is not perfect, namely when describing more limited interactions [40] (limited to a given molecule) or when screening is important. However, we will use it as a first approximation that provides a first estimate for the parameter η. In the frame of the homogeneous model, the dielectric susceptibility reads

$$\tilde{\tilde{\chi}} = \frac{\chi_0}{k^2 + \mathcal{L}(\omega)}, \tag{A3}$$

which makes the dependency of the permittivity on the wave vector explicit. This function is the Fourier transform of $\tilde{\tilde{\chi}}$ with respect to space and time.

When the assumption $\mathrm{Re}[\sqrt{\mathcal{L}(\omega)}] > 0$ holds, [1] the inverse Fourier transform of Eq. (A3) with respect to space is

$$\tilde{\chi}(\mathbf{r},\omega) = \frac{\chi_0}{4\pi r} e^{-r\sqrt{\mathcal{L}(\omega)}}. \tag{A4}$$

The nonlocality extents over a range directly linked to $\mathrm{Re}[\sqrt{\mathcal{L}(\omega)}]$. Therefore, we define the mean interaction radius R as

$$R = \frac{1}{\mathrm{Re}[\sqrt{\mathcal{L}(\omega)}]}. \tag{A5}$$

4. Derivation of the spatial dispersion coefficient

Once the model and the definition of η are known, it is a simple exercise to compute η when $k_x = 0$ and $k_y = 0$, taking into account that $\beta_0^2 = k^2 = k_x^2 + k_y^2 + k_z^2$. We obtain

$$\eta = \frac{\omega^2}{c^2}\chi_0 \frac{1}{\left[k^2 + \mathcal{L}(\omega)\right]^3}, \tag{A6}$$

where $\beta_0 = k = k_z$.

5. Left-handed material in the E, D, B approach

The modeling of media with spatial dispersion is easier to perform in the E, D, B approach [41,42], in which the magnetic and the electric responses of the material are fully contained in the generalized electromagnetic susceptibility

$$\tilde{\tilde{\chi}}^{(1)} = n^2(\vec{k},\omega) - 1. \tag{A7}$$

It is, therefore, important to determine how the usual definition of a left-handed material in a nonchiral material transposes to our model. It is usually stated that left-handed metamaterial verifies

$$\mathrm{Re}[\mu(\omega)] < 0, \tag{A8}$$

$$\mathrm{Re}[\varepsilon(\omega)] < 0. \tag{A9}$$

However, in our model, μ and ε are not defined. Only their product appears in the definition of the refractive index

$$\varepsilon_r \mu_r = n^2(\mathbf{k},\omega) = 1 + \tilde{\chi}^{(1)} = \frac{c^2}{\omega^2}k^2. \tag{A10}$$

With the definitions

$$\varepsilon_r = 1 + \tilde{\chi}_e(\omega), \tag{A11}$$

$$\mu_r = 1 + \tilde{\chi}_h(\omega) = [1 - \tilde{\chi}_b(\omega)]^{-1} \tag{A12}$$

introduced in Eq. (A10), the classical electric and magnetic parts can be retrieved from

$$\tilde{\tilde{\chi}}^{(1)}(\mathbf{k},\omega) = \tilde{\chi}_e(\omega) + k^2\left[\frac{c^2}{\omega^2}\tilde{\chi}_b(\omega)\right], \tag{A13}$$

$$\tilde{\chi}_e(\omega) = \tilde{\tilde{\chi}}^{(1)}(0,\omega), \tag{A14}$$

[1] In this case, the exponential is decreasing at (positive) infinity. Indeed, as two square roots exist, we can always choose the one corresponding to $\mathrm{Re}[\sqrt{a}] > 0$. The only exception would be when $\mathrm{Re}[\sqrt{a}] = 0$. In this case, the integral defining the Fourier transform would be undefined.

$$\tilde{\chi}_b(\omega) = \frac{\omega^2}{2c^2} \left. \frac{\partial^2 \tilde{\chi}^{(1)}}{\partial k^2} \right|_{k=0}. \tag{A15}$$

From these relations, a nonchiral left-handed material should verify

$$\mathrm{Re}[1 + \tilde{\chi}^{(1)}(0,\omega)] < 0, \tag{A16}$$

$$\mathrm{Re}\left[1 - \frac{\omega^2}{2c^2} \left. \frac{\partial^2 \tilde{\chi}^{(1)}}{\partial k^2} \right|_{k=0} k^2\right] < 0. \tag{A17}$$

If the structure under consideration presents chirality, the LHM should be defined as having opposite signs for the phase velocity and the group velocity, i.e., $\mathrm{Re}[\frac{k}{\omega}]\mathrm{Re}[\frac{\mathrm{d}k}{\mathrm{d}\omega}] < 0$.

6. Left-handed material with homogeneous nonlocal response

In the particular case, where

$$\tilde{\chi}^{(1)} = \frac{\chi_0}{k^2 + \mathcal{L}(\omega)}, \tag{A18}$$

the inequalities satisfied in a left-handed material are, therefore,

$$1 + \mathrm{Re}\left[\frac{\chi_0}{\mathcal{L}(\omega)}\right] < 0, \tag{A19}$$

$$1 + \frac{\omega^2}{c^2}\mathrm{Re}\left[\frac{\chi_0}{\mathcal{L}^2(\omega)}\right] < 0. \tag{A20}$$

We should remember the previous assumption that

$$\mathrm{Re}[\sqrt{\mathcal{L}(\omega)}] > 0. \tag{A21}$$

7. Lorentz resonance

We evaluate the range of parameters near a Lorentz resonance defined by the frequency ω_r and the losses γ_r:

$$\mathcal{L}(\omega) = \kappa\left(\omega_\mathrm{r}^2 - \omega^2 - i\gamma_\mathrm{r}\omega\right) \tag{A22}$$

$$= a + ib. \tag{A23}$$

With the help of this definition, inequalities (A19) to (A21) lead to

$$\chi_0 > 0, \tag{A24}$$

$$\left(\omega_\mathrm{r}^2 - \omega^2\right)^2 < (\gamma_\mathrm{r}\omega)^2, \tag{A25}$$

$$\kappa\left(\omega_\mathrm{r}^2 - \omega^2\right) < 0, \tag{A26}$$

$$\kappa\gamma_\mathrm{r}\omega \neq 0. \tag{A27}$$

From these inequalities and the definition of the nonlocality radius, we conclude that the magnitude of both χ_0 and R have no maximal values.

8. Nonlocal behavior on a wavelength scale

It is important to determine how R compares to the wavelength λ in the range of values defined by inequalities (A24) to (A27).

As we assume that we are working near the frequency resonance,

$$\omega \approx \omega_\mathrm{r}, \tag{A28}$$

$$k \approx \frac{\omega_\mathrm{r}}{c} n_L. \tag{A29}$$

For a sharp resonance, $\gamma_\mathrm{r} \ll \omega_\mathrm{r}$, so that

$$|\omega - \omega_\mathrm{r}| \ll \gamma_\mathrm{r}, \tag{A30}$$

and, therefore,

$$|\mathcal{L}(\omega)| = |a + ib| \ll |\kappa|\omega_\mathrm{r}^2. \tag{A31}$$

The usual choice for κ is

$$|\kappa| = \frac{1}{c^2}, \tag{A32}$$

which implies

$$|\mathcal{L}(\omega)| \ll \frac{\omega_\mathrm{r}^2}{c^2} \approx \frac{k^2}{n_L^2}. \tag{A33}$$

Near the resonance, it can, therefore, be assumed that

$$\tilde{\chi}(k,\omega) \approx \frac{\chi_0}{k^2}, \tag{A34}$$

$$|b| \approx \left|\gamma_\mathrm{r}\frac{\omega_\mathrm{r}}{c^2}\right| \ll \frac{\omega_\mathrm{r}^2}{c^2}, \tag{A35}$$

$$2\left|\frac{a}{b}\right| \approx \frac{\omega_\mathrm{r} - \omega}{\gamma_\mathrm{r}} \ll 1. \tag{A36}$$

From this last inequality, we deduce that $|a| \ll 2|b|$ and, therefore, that

$$\frac{1}{R} \approx \sqrt{i\,b} = \frac{\sqrt{|b|}}{\sqrt{2}}, \tag{A37}$$

$$R^2 \approx \frac{2}{|b|} \approx \frac{2c^2}{\gamma_\mathrm{r}\omega_\mathrm{r}} \gg \frac{2}{k_\mathrm{r}^2}. \tag{A38}$$

In the frame of the homogeneous model, the value of R depends strongly on the width of the resonance γ_r. The last inequality shows that this model can take into account large structures. It provides a value for the parameter η approximately given by

$$\eta \approx \frac{\omega_\mathrm{r}^2}{c^2}\frac{\chi_0}{k^6} \approx \frac{\tilde{\chi}}{k_\mathrm{r}^2} = \frac{n_r^2 - 1}{k_\mathrm{r}^2}, \tag{A39}$$

where k_r and n_r are the wave vector and the refractive index near resonance. In a left-handed material, we must have $n_r = n_L < 0$.

Practical values for η will therefore vary between a few percents of k_r^{-2}, when $|n| \approx 1$, and can reach values around k_r^{-2} when $|n_r| \approx \sqrt{2}$.

9. Effective spatial dispersion coefficient in the mean-field model

As was stated in [15], if we define the finesse of the cavity by $\mathcal{F}$ and the thickness of the left-handed medium by l_L, and we assume that the right-handed medium is a classical material with negligible spatial dispersion, then the effective dispersion coefficient in the mean-field model is given by

$$\theta = \frac{\mathcal{F}}{4\pi}\frac{l_L\,\eta_L}{k_L} = -\frac{\mathcal{F}}{4\pi\,k}\frac{l_L\,\eta_L}{|n_L|}. \tag{A40}$$

In reduced units, we define $\bar{\theta} = \theta\, k^4$ and $\bar{\eta} = \eta\, k^2$, so that

$$\bar{\theta} = -\frac{\mathcal{F}}{4\pi}\, k\, \frac{l_L\, \bar{\eta}_L}{|n_L|}. \tag{A41}$$

Therefore, when

$$\eta \approx \frac{n_r^2 - 1}{k_r^2}, \tag{A42}$$

we find

$$\bar{\theta} \approx -\frac{\mathcal{F}}{2}\, \frac{n_L^2 - 1}{|n_L|}\, \frac{l_L}{\lambda_L} \approx \left(1 - n_L^2\right) \frac{\mathcal{F}}{2}\, \frac{l_L}{\lambda_L}. \tag{A43}$$

For values of $\mathcal{F}\, l_L/\lambda_L \approx 100$, $\bar{\theta}$ will be of magnitude 0.1–1, provided that $n_L^2 \approx 1$.

[1] A. Boardman, M. Brongersma, M. Stockman, and M. Wegener, J. Opt. Soc. Am. B **26**, PM1 (2009).

[2] R. A. Shelby, D. R. Smith, S. C. Nemat-Nasser, and S. Schultz, Appl. Phys. Lett. **78**, 489 (2001).

[3] C. G. Parazzoli, R. B. Greegor, K. Li, B. E. C. Koltenbah, and M. Tanielian, Phys. Rev. Lett. **90**, 107401 (2003).

[4] A. A. Houck, J. B. Brock, and I. L. Chuang, Phys. Rev. Lett. **90**, 137401 (2003).

[5] D. R. Smith, J. B. Pendry, and M. C. K. Wiltshire, Science **305**, 788 (2004).

[6] K. Aydin, K. Guven, M. Kafesaki, L. Zhang, C. M. Soukoulis, and E. Ozbay, Opt. Lett. **29**, 2623 (2004).

[7] C. Enkrich, M. Wegener, S. Linden, S. Burger, L. Zschiedrich, F. Schmidt, J. F. Zhou, Th. Koschny, and C. M. Soukoulis, Phys. Rev. Lett. **95**, 203901 (2005).

[8] T. F. Gundogdu, I. Tsiapa, A. Kostopoulos, G. Konstantinidis, N. Katsarakis, R. S. Penciu, M. Kafesaki, E. N. Economou, T. Koschny, and C. M. Soukoulis, Appl. Phys. Lett. **89**, 084103 (2006).

[9] A. A. Zharov, N. A. Zharova, I. V. Shadrivov, and Y. S. Kivshar, Appl. Phys. Lett. **87**, 091104 (2005).

[10] G. D'Aguanno, N. Mattiucci, M. Scalora, and M. J. Bloemer, Phys. Rev. Lett. **93**, 213902 (2004).

[11] V. M. Shadrivov, A. A. Zharov, and Y. S. Kivshar, J. Opt. Soc. Am. B **23**, 529 (2006).

[12] I. Kourakis, N. Lazarides, and G. P. Tsironis, Phys. Rev. E **75**, 067601 (2007).

[13] P. Kockaert, P. Tassin, G. Van der Sande, I. Veretennicoff, and M. Tlidi, Phys. Rev. A **74**, 033822 (2006).

[14] L. Gelens, G. Van der Sande, P. Tassin, M. Tlidi, P. Kockaert, D. Gomila, I. Veretennicoff, and J. Danckaert, Phys. Rev. A **75**, 063812 (2007); L. Gelens, D. Gomila, G. Van der Sande, J. Danckaert, P. Colet, and M. A. Matías, *ibid.* **77**, 033841 (2008).

[15] P. Kockaert, P. Tassin, I. Veretennicoff, G. Van der Sande, and M. Tlidi, J. Opt. Soc. Am. B **26**, B148 (2009).

[16] L. A. Lugiato and R. Lefever, Phys. Rev. Lett. **58**, 2209 (1987).

[17] D. Gomila, A. J. Scroggie, and W. J. Firth, Physica D **227**, 70 (2007).

[18] A. J. Scroggie *et al.*, Chaos Solitons Fractals **4**, 1323 (1994).

[19] V. B. Taranenko, K. Staliunas, and C. O. Weiss, Phys. Rev. A **56**, 1582 (1997); Phys. Rev. Lett. **81**, 2236 (1998); S. Barland *et al.*, Nature (London) **419**, 699 (2002).

[20] U. Bortolozzo, L. Pastur, P. L. Ramazza, M. Tlidi, and G. Kozyreff, Phys. Rev. Lett. **93**, 253901 (2004); M. G. Clerc, A. Petrossian, and S. Residori, Phys. Rev. E **71**, 015205 (2005); F. Haudin, R. G. Rojas, U. Bortolozzo, M. G. Clerc, and S. Residori, Phys. Rev. Lett. **106**, 063901 (2011).

[21] F. Leo *et al.*, Nat. Photonics **7**, 471 (2010).

[22] K. Staliunas and V. J. Sanchez-Morcillo, *Transverse Patterns in Nonlinear Optical Resonators* (Springer-Verlag, Berlin, 2003); Y. S. Kivshar and G. P. Agrawal, *Optical Solitons: From Fiber to Photonic Crystals* (Academic Press, Elsevier, Amsterdam, 2003).

[23] M. Tlidi, M. Taki, and T. Kolokolnikov, Chaos **17**, 037101 (2007).

[24] N. Akhmediev and A. Ankiewicz, *Dissipative Solitons: From Optics to Biology and Medicine* (Springer-Verlag, Berlin, 2008).

[25] T. Ackemann, W. J. Firth, and G. L. Oppo, J. Phys. B **57**, 323 (2009).

[26] H. G. Purwins, H. U. Bodeker, and S. Amiranashvili, Adv. Phys. **59**, 485 (2010).

[27] K. Staliunas, R. Herrero, and G. J. de Valcárcel, Phys. Rev. E **73**, 065603 (2006).

[28] K. Staliunas, O. Egorov, Y. S. Kivshar, and F. Lederer, Phys. Rev. Lett. **101**, 153903 (2008); O. A. Egorov, F. Lederer, and K. Staliunas, Phys. Rev. A **82**, 043830 (2010).

[29] P. Ding, E. J. Liang, W. Q. Hu, L. Zhang, Q. Zhou, and Q. Z. Xue, Photonics and Nanostructures **7**, 92 (2009).

[30] U. Ritschel, L. Wilets, J. J. Rehr, and M. Grabiak, J. Phys. G **18**, 1889 (1992).

[31] Lendert Gelens, Ph.D. thesis, Vrije Universiteit Brussel, 2010.

[32] J. Burke and E. Knobloch, Chaos **17**, 037102 (2007).

[33] P. D. Woods and A. R. Champneys, Physica D **129**, 147 (1999).

[34] M. Tlidi and L. Gelens, Opt. Lett. **35**, 306 (2010).

[35] Y.-P. Ma, J. Burke, and E. Knobloch, Physica D **239**, 1867 (2010).

[36] D. J. B. Lloyd, B. Sandstede, D. Avitabile, and A. R. Champneys, SIAM J. App. Dyn. Syst. **7**, 1049 (2008).

[37] V. Agranovich and V. Ginzburg, *Progress in Optics*, edited by Emil Wolf (North-Holland, Amsterdam, 1971), Vol. IX.

[38] V. Agranovich and V. Ginzburg, *Progress in Optics*, edited by Emil Wolf (North-Holland, Amsterdam, 1977), Vol. XV.

[39] U. Ritschel, L. Wilets, J. J. Rehr, and M. Grabiak, J. Phys. G: Nucl. Part. Phys. **18**, 1889 (1992).

[40] R. W. Schoonover, J. M. Rutherford, O. Keller, and P. S. Carney, Phys. Lett. A **342**, 363 (2005).

[41] V. M. Agranovich, Y. R. Shen, R. H. Baughman, and A. A. Zakhidov, Phys. Rev. B **69**, 165112 (2004).

[42] K. Cho, J. Phys. Condens. Matter **20**, 175202 (2008).